



 Cite this: *RSC Adv.*, 2020, 10, 4286

Synthesis of a GaOOH/ZnBiTaO₅ heterojunction photocatalyst with enhanced photocatalytic performance toward enrofloxacin

 Panqi Huang ^b and Jingfei Luan^{*ab}

In this work, a GaOOH/ZnBiTaO₅ heterojunction photocatalyst was synthesized innovatively and characterization techniques including XRD, SEM-EDS, XPS, FT-IR, PL and UV-Vis DRS were carried out to analyse the structural and morphological properties of the GaOOH/ZnBiTaO₅ heterojunction photocatalyst. The GaOOH is dispersed on the surface of ZnBiTaO₅ to form a heterojunction structure according to the SEM image. The band gaps of 10 wt%, 25 wt% and 50 wt% GaOOH/ZnBiTaO₅ heterojunction photocatalysts were calculated to be 3.21 eV, 3.22 eV and 3.23 eV, respectively, which were between the band gaps of pure ZnBiTaO₅ (3.19 eV) and pure GaOOH (4.76 eV). The photocatalytic performance of the GaOOH/ZnBiTaO₅ heterojunction photocatalyst was investigated by degrading enrofloxacin under ultraviolet light. The results showed that the as-prepared 25 wt% GaOOH/ZnBiTaO₅ presented optimal photocatalytic performance and could remove 58.27% of enrofloxacin in 60 min, which was higher than that of pure ZnBiTaO₅ (53.7%) and pure GaOOH (35.4%). In addition, it was confirmed that $\cdot\text{O}_2^-$, h^+ and $\cdot\text{OH}$ were all the active radicals during the degradation process. Finally, the possible degradation mechanism of enrofloxacin was discussed in detail. This work provided a viable strategy for improving the photocatalytic performance of wide band gap semiconductors.

 Received 21st November 2019
 Accepted 18th January 2020

DOI: 10.1039/c9ra09741d

rsc.li/rsc-advances

Introduction

Recently, water pollution caused by the extensive use of antibiotics has become one of the most urgent problems to solve. In many advanced oxidation methods, photocatalysis technology is an effective, environmentally friendly and low-cost method for treating environmental pollutants.^{1–8} Up to now, a large number of semiconductor materials, such as metal oxides (Bi₁₂TiO₂₀, K₆Nb_{10.8}O₃₀, BiVO₄),^{9–11} have been identified as active photocatalysts. However, there are still some shortcomings that hinder the practical application of photocatalytic technology, which makes it necessary to design new photocatalysts to increase their potential for practical applications.^{12,13}

Among many types of metal oxides, mixed oxides, have been found to have good photocatalytic properties.^{14–19} According to the previous reports, many polymetallic compounds that had a pyrochlore-type structure, such as Bi₂InTaO₇,²⁰ Ca₂Nb₂O₇,²¹ Y₂GdSbO₇ (ref. 22) and ZnFe₂O₄,²³ showed good photocatalytic properties toward organic contaminants. Carta *et al.* prepared CoAl₂O₄ films and verified their high photocatalytic activity.²⁴ Cui *et al.* also successfully synthesized ZnCo₂O₄ nanoparticles

which could degrade the methyl blue dye solution with high efficiency under light irradiation.²⁵

However, a single photocatalyst had some inherent properties and its practical application was limited. Therefore, the construction of a heterojunction photocatalyst became an effective method for improving the efficiency and stability of the photocatalyst.^{26–29} For example, Yang *et al.* synthesized a novel hierarchical Co₃O₄/Bi₂O₂CO₃ heterojunction composite photocatalyst, which had enhanced photocatalytic activity for degrading methyl orange dye solution under visible light irradiation.³⁰

Furthermore, GaOOH was a wide band gap metal hydroxide semiconductor and commonly was used as a precursor for the preparation of Ga₂O₃.³¹ According to previous reports, GaOOH nanorods had significant photocatalytic activity for the degradation of aromatic compounds.³² On the one hand, the original unit cell of GaOOH was composed of twisted octahedral GaO₆, which could generate a strong dipole moment, thereby promoting the separation of photogenerated electrons and photogenerated holes.^{33,34} On the other hand, the low potential of the valence band gave GaOOH a high oxidizing power for various photocatalytic reactions.³⁵

Therefore, ZnBiTaO₅ with a pyrochlore-type structure was prepared by solid-state reaction method for the first time in this paper. At the same time, the GaOOH/ZnBiTaO₅ heterojunction photocatalyst was constructed by solvothermal method in this paper. The characterizations including X-ray diffraction (XRD),

^aSchool of Physics, Changchun Normal University, Changchun, Jilin, 130032, China

^bState Key Laboratory of Pollution Control and Resource Reuse, School of the Environment, Nanjing University, Nanjing, 210023, China. E-mail: jfluan@nju.edu.cn


scanning electron microscopy-X-ray energy dispersion spectroscopy (SEM-EDS), X-ray photoelectron spectroscopy (XPS), Fourier transform infrared spectroscopy (FT-IR), UV-visible diffuse reflectance spectroscopy (UV-Vis DRS) were used to analyse the morphology, chemical state, band gap and structure of GaOOH/ZnBiTaO₅ heterojunction photocatalyst. Moreover, the enrofloxacin was used to test the photocatalytic performance of GaOOH/ZnBiTaO₅ heterojunction photocatalyst. The three-dimensional fluorescence was used to visualize the changes of enrofloxacin in degradation process. The hydroxyl radicals and superoxide radicals which generated in photocatalytic process were determined by the electron paramagnetic resonance spectrometer (EPR). Finally, three possible degradation pathways of enrofloxacin were analysed in detail.

Experimental

The pure ZnBiTaO₅ was synthesised by solid-state reaction method. The raw materials, ZnO, Bi₂O₃ and Ta₂O₅ with purity of 99.99% (Sinopharm Group Chemical Reagent Co., Ltd., Shanghai, China), were weighed according to an atomic ratio of 1 : 1 : 1 (Zn : Bi : Ta). The calcination was carried out at 900 °C for 25 h in an electric furnace (KSL 1700X, Hefei Kejing Materials Technology Co., Ltd., Hefei, China).

GaOOH/ZnBiTaO₅ heterojunction photocatalyst was synthesised by solvothermal method. 1.1296 g Ga₂O₃ powder with a purity of 99.99% (Aladdin Biochemical Technology Co., Ltd., Shanghai, China) was weighed accurately and the pure ZnBiTaO₅ powder was weighed according to demand, then they were placed in a beaker and 80 mL of deionized water and 80 mL of absolute ethanol were added. The mass percentages of GaOOH to ZnBiTaO₅ were set to be 10%, 25%, and 50%, respectively. Then the solution was transferred into a 200 mL tetrafluoro-lined reactor and heated at 200 °C for 12 h. In addition, the pure GaOOH was synthesised as a control sample according to the above procedures with no ZnBiTaO₅ powder added.

The crystal structure of sample was analysed by the powder X-ray diffractometer (XRD, D/MAX-RB, Rigaku Corporation, Japan) with CuK α radiation ($\lambda = 1.54056$). The data was collected using Step-scan program at 295 K and the scan range was 10–80°. The morphological feature of sample was analysed by scanning electron microscopy-X-ray energy dispersion spectroscopy (SEM-EDS, LEO 1530VP, LEO Corporation, Dresden, Germany). The morphology and the diffraction lattice of sample were analysed by the transmission electron microscopy (TEM, Tecnai F20 S-Twin, FEI Corporation, Hillsboro, OR, USA). The element contents of sample were analysed by the X-ray photoelectron spectroscopy (XPS, ESCALABMK-2, VG Scientific Ltd., London, UK). The main chemical vibrational specie of sample was analysed by the fourier transform infrared spectrometer (Nexus, Nicolet Corporation, Madison, WI, USA) with an attenuated total reflectance (ATR) mode. The UV-visible diffuse reflectance spectra of samples were analysed by UV-Vis spectrophotometer (UV-2450, Shimadzu Corporation, Kyoto, Japan) and the background material was pure BaSO₄ powder. The superoxide radicals ($\cdot\text{O}_2^-$) and hydroxyl radicals ($\cdot\text{OH}$)

generated during photocatalytic degradation of enrofloxacin were determined by electron paramagnetic resonance spectrometer (EPR, EMX-10/12, Bruker, Germany).

Enrofloxacin was selected to evaluate the photocatalytic performance of GaOOH/ZnBiTaO₅. The photocatalytic experiments were carried out in a photocatalytic reactor (Xujiang Machine, Nanjing, China) which contained a mercury lamp (500 W) with major emission wavelength of 365 nm, optical filters ($\lambda < 400$ nm) and a magnetic stirring device. The photocatalyst dosage was set to be 1 g L⁻¹ and the initial concentration of enrofloxacin was set to be 10 mg L⁻¹. In the procedure of photocatalytic degradation, 2 mL of the solution was taken under ultraviolet light for 10 min, 20 min, 30 min, 40 min, and 60 min, and the absorbance of enrofloxacin was measured at 276 nm using the UV-visible spectrophotometer (UV-2550, Shimadzu Corporation, Kyoto, Japan). The total organic carbon (TOC) concentration was determined by the TOC analyser (TOC-5000, Shimadzu Corporation). The three-dimensional fluorescence of enrofloxacin was determined by the full-function fluorescence spectrometer (Fluoromax-4, Horiba Scientific). According to our previous report, the relationship between the absorbance and the concentration for enrofloxacin matched the eqn (1).³⁶ In addition, the removal rate of enrofloxacin ($D\%$) was counted by the eqn (2).

$$A = 0.10632 \times C + 0.01381 \quad (1)$$

$$D\% = (C_0 - C_t)/C_0 \times 100\% \quad (2)$$

where, A was the absorbance of enrofloxacin at 276 nm, C was the concentration of enrofloxacin, $D\%$ was the removal rate of enrofloxacin, C_0 was the initial concentration of enrofloxacin, and C_t was the concentration of enrofloxacin at time t .

Results and discussion

Structure and morphology analysis

The crystal structures of as-prepared samples were analysed by XRD, as shown in Fig. 1. Fig. 1(a) shows the Pawley refinements of the as-prepared ZnBiTaO₅. The raw XRD data of the as-prepared ZnBiTaO₅ was refined in this paper by using the Materials Studio software, which was based on Pawley analysis. There was a good agreement between the observed and calculated data for the as-prepared ZnBiTaO₅, indicating that the as-

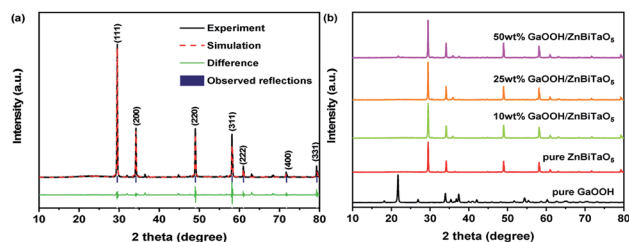


Fig. 1 The Pawley refinements of pure ZnBiTaO₅ (a); the XRD patterns of pure ZnBiTaO₅, pure GaOOH and 10 wt%, 25 wt% and 50 wt% GaOOH/ZnBiTaO₅ heterojunction photocatalysts (b).



prepared ZnBiTaO₅ was a single phase and had high crystallinity. According to the refinements results, the as-prepared ZnBiTaO₅ crystallized with a pyrochlore-type structure, a cubic crystal system and a space group *Fm* $\bar{3}$ *m* (O atom was included in the model). The lattice parameter of the as-prepared ZnBiTaO₅ was calculated to be 5.268012 Å. In addition, the diffraction peaks at 29.51°, 34.18°, 49.03°, 58.18°, 61.03°, 71.75° and 79.34° were corresponding with the (111), (200), (220), (311), (222), (400) and (331) planes of pure ZnBiTaO₅, respectively, which were all marked in the Fig. 1(a). Fig. 1(b) shows the XRD patterns of pure ZnBiTaO₅, pure GaOOH and 10 wt%, 25 wt% and 50 wt% GaOOH/ZnBiTaO₅ heterojunction photocatalysts. According to the Fig. 1(b), it could be observed that there were both strong diffraction peaks of pure ZnBiTaO₅ and weak diffraction peaks of pure GaOOH in the XRD data of 10 wt%, 25 wt% and 50 wt% GaOOH/ZnBiTaO₅ heterojunction photocatalysts, indicating that the 10 wt%, 25 wt% and 50 wt% GaOOH/ZnBiTaO₅ heterojunction photocatalysts were prepared successfully.

The morphology and elemental composition of samples were analysed by SEM-EDS. Fig. 2 shows the SEM pictures of pure ZnBiTaO₅, pure GaOOH, 10 wt%, 25 wt% and 50 wt% GaOOH/ZnBiTaO₅ heterojunction photocatalysts and the EDS data of 25 wt% GaOOH/ZnBiTaO₅ heterojunction photocatalyst. It could be confirmed that 10 wt%, 25 wt% and 50 wt% GaOOH/ZnBiTaO₅ heterojunction photocatalysts were prepared successfully because both ZnBiTaO₅ and GaOOH were observed in Fig. 2(c, d and e). According to the Fig. 2(c, d and e), GaOOH covered the surface of ZnBiTaO₅ to form a heterojunction structure. In Fig. 2(f), the EDS results of GaOOH/ZnBiTaO₅ heterojunction photocatalyst showed that there were no impure elements in GaOOH/ZnBiTaO₅ heterojunction photocatalyst.

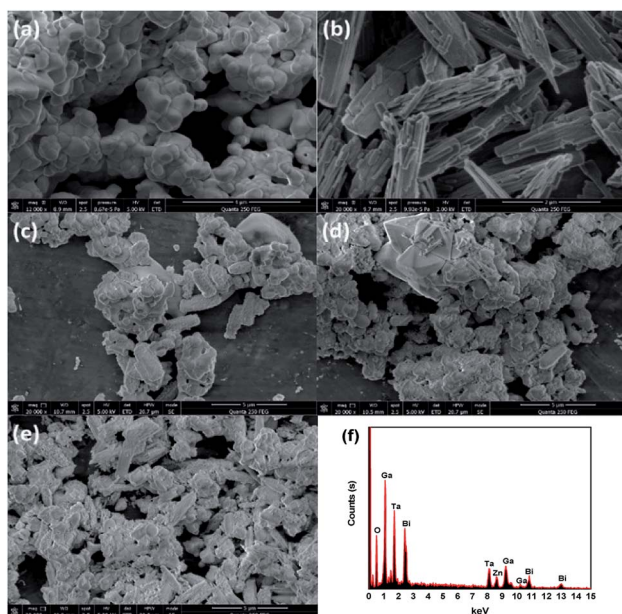


Fig. 2 The SEM pictures of pure ZnBiTaO₅, pure GaOOH, 10 wt%, 25 wt% and 50 wt% GaOOH/ZnBiTaO₅ heterojunction photocatalysts (a–e); the EDS spectra of 25 wt% GaOOH/ZnBiTaO₅ heterojunction photocatalyst (f).

Band structure and chemical state analysis

Fig. 3 shows the UV-vis DRS spectra and band gaps of pure ZnBiTaO₅, pure GaOOH and 10 wt%, 25 wt% and 50 wt% GaOOH/ZnBiTaO₅ heterojunction photocatalysts. As shown in Fig. 3(a), compared with the pure GaOOH, the absorption edges of 10 wt%, 25 wt% and 50 wt% GaOOH/ZnBiTaO₅ heterojunction photocatalysts all presented apparent red-shift phenomenon. The absorbance was counted by using the Kubelka–Munk transformation method in this paper. The optical absorption near the band edge of the crystalline semiconductors follows the eqn (3).^{37,38}

$$\alpha h\nu = A(h\nu - E_g)^n \quad (3)$$

where α , ν , E_g , and A are absorption coefficient, light frequency, band gap, and proportional constant, respectively. In this formula, n determines the type of the transition in a semiconductor. Therefore, according to the eqn (3), it could be obtained that the band gaps of 10 wt%, 25 wt% and 50 wt% GaOOH/ZnBiTaO₅ heterojunction photocatalysts were counted to be 3.21 eV, 3.22 eV and 3.23 eV, respectively, which were shown in Fig. 3(b). The band gaps of pure ZnBiTaO₅ and pure GaOOH were counted to be 3.19 eV and 4.76 eV, respectively, which were shown in Fig. 3(c) and (d). According to the UV-vis DRS results, the band gaps of 10 wt%, 25 wt% and 50 wt% GaOOH/ZnBiTaO₅ heterojunction photocatalysts were close to that of pure ZnBiTaO₅, but they were much lower than that of pure GaOOH. In addition, the counted values of n were all 0.5 for all as-prepared samples, indicating that the optical transition of all samples belonged to the type of direct transition.³⁹

Fig. 4(a) shows the FT-IR spectra of GaOOH/ZnBiTaO₅. According to the Fig. 4(a), the peaks that belonged to GaOOH were observed in the FT-IR spectra of 10 wt%, 25 wt% and 50 wt% GaOOH/ZnBiTaO₅ heterojunction photocatalysts. It

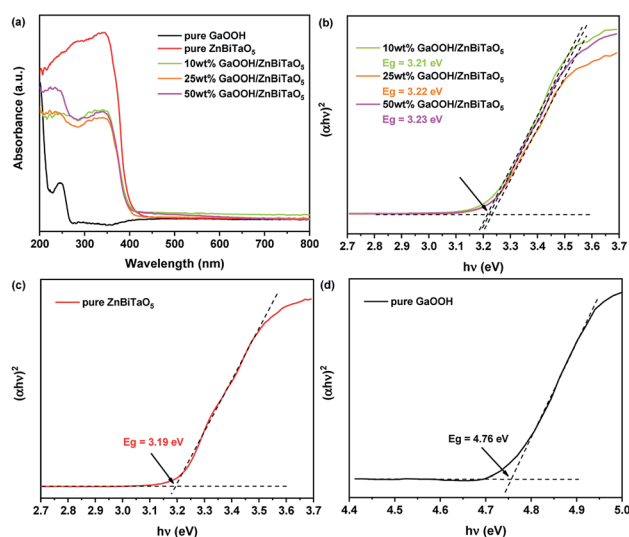


Fig. 3 The UV-vis DRS spectra of all photocatalysts (a); the band gaps of 10 wt%, 25 wt% and 50 wt% GaOOH/ZnBiTaO₅ heterojunction photocatalysts (b); the band gaps of pure ZnBiTaO₅ (c) and pure GaOOH (d)



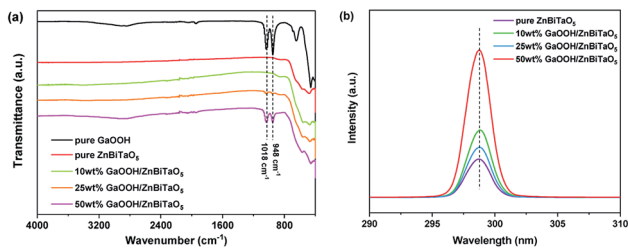


Fig. 4 The FT-TR spectra (a) and PL spectra (b) of GaOOH/ZnBiTaO₅ heterojunction photocatalyst.

could be seen from Fig. 4(a) that with the increasing composite amount of GaOOH, the peak intensity at 1018 cm⁻¹ and 948 cm⁻¹ became more and more stronger and the two peaks were attributed to the constitutional Ga–OH bending mode and its overtones in GaOOH.^{40,41} The FT-IR results revealed indirectly the successful preparation of GaOOH/ZnBiTaO₅ heterojunction photocatalyst. Fig. 4(b) shows the PL spectra of GaOOH/ZnBiTaO₅. In general, the higher intensity of emission peak in PL spectra revealed the higher recombination rate of electrons–holes pairs in photocatalyst. The construction of GaOOH/ZnBiTaO₅ heterojunction increased the recombination rate of electrons–holes pairs for ZnBiTaO₅, according to the Fig. 4(b). In addition, the intensity of emission peaks for 25 wt% GaOOH/ZnBiTaO₅ heterojunction was lowest. Thus, the optimum composite amount of GaOOH in GaOOH/ZnBiTaO₅ heterojunction was considered to 25 wt%, according to the results of PL spectra.

The XPS spectra was obtained to analyse the oxidation state and the surface chemical composition of samples. Fig. 5 shows XPS spectra of Zn2p, Bi4f, Ta4f and Ga3d for 25 wt% GaOOH/ZnBiTaO₅ heterojunction photocatalyst. The peaks at the binding energies of 1022.0 eV and 1045.0 eV in Fig. 5(a) were corresponding to Zn2p_{3/2} and Zn2p_{1/2}, respectively, which revealed

that the chemical valence of Zn element was +2.^{42,43} In Fig. 5(b), the binding energies at 159.0 eV and 163.7 eV were attributed to Bi4f_{7/2} and Bi4f_{5/2}, respectively, and the chemical valence of Bi element was confirmed to be +3.^{44,45} In Fig. 5(c), the three peaks of Ta4f were appeared at the binding energies of 20.3 eV (Ta4f_{7/2}), 25.1 eV (Ta4f_{5/2}) and 26.5 eV (Ta4f_{3/2}), which indicated that the chemical valence of Ta element was +5.^{46,47} Moreover, in Fig. 5(d), the binding energies of 19.7 eV and 20.7 eV were all corresponded to Ga3d_{3/2} and the binding energies of 25.0 eV and 26.5 eV were all corresponded to Ga3d_{5/2}, thus the chemical valence of Ga element was +3.^{48,49}

Photocatalytic performance test

Fig. 6 shows the removal of enrofloxacin under ultraviolet light irradiation with TiO₂, pure ZnBiTaO₅, pure GaOOH, 10 wt% GaOOH/ZnBiTaO₅, 25 wt% GaOOH/ZnBiTaO₅ or 50 wt% GaOOH/ZnBiTaO₅ as a photocatalyst. As shown in Fig. 6(a), when the 10 wt%, 25 wt% or 50 wt% GaOOH/ZnBiTaO₅ was used as a photocatalyst, after ultraviolet light irradiation for 60 min, the removal rate of enrofloxacin was 57.02%, 58.27% or 54.55%, which was higher than that of pure ZnBiTaO₅ (53.7%), pure GaOOH (35.4%), or TiO₂ (29.37%). In addition, the photocatalytic kinetics of enrofloxacin degradation in this paper could be analysed using the Langmuir–Hinshelwood (L–H) model (eqn (4)).⁵⁰ Due to the initial concentration of enrofloxacin in this paper was 10 mg L⁻¹, (1 + K_c) could be assumed to be equal to 1. Thus, eqn (4) could be expressed in the form of eqn (5), where k' was the pseudo first-order rate constant. After integrating eqn (5) and (6) was obtained.

$$r = -dc/dt = \kappa\theta = \kappa Kc/(1 + Kc) \quad (4)$$

$$-dc/dt = \kappa Kc = k'c \quad (5)$$

$$\ln(c/c_0) = -k't \quad (6)$$

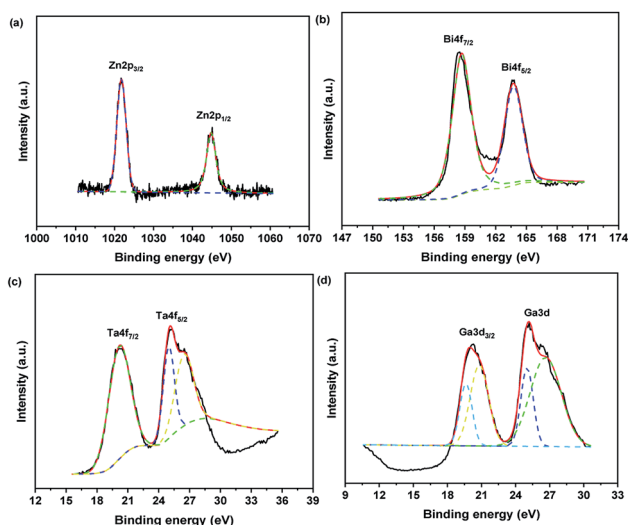


Fig. 5 The XPS spectra of Zn2p (a), Bi4f (b), Ta4f (c) and Ga3d (d) for 25 wt% GaOOH/ZnBiTaO₅ heterojunction photocatalyst.

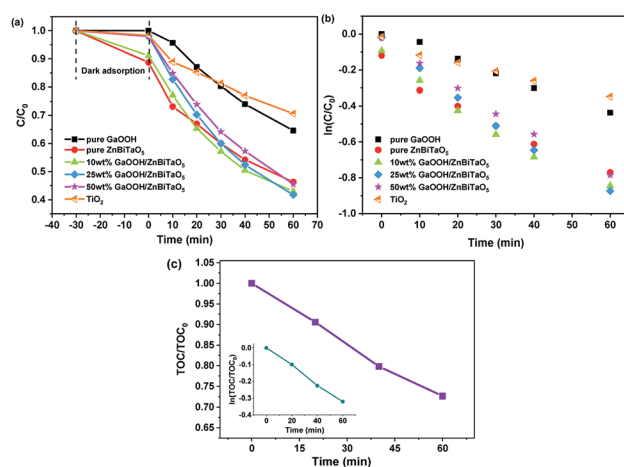


Fig. 6 The removal rate (a) and removal kinetics (b) of enrofloxacin with TiO₂, pure ZnBiTaO₅, pure GaOOH, 10 wt%, 25 wt% and 50 wt% GaOOH/ZnBiTaO₅ as a photocatalyst; the mineralization rate of enrofloxacin with 25 wt% GaOOH/ZnBiTaO₅ as a photocatalyst (c).



where r is reaction rate, c is the concentration of enrofloxacin, c_0 is the initial concentration of enrofloxacin, t is the irradiation time, κ is the reaction rate constant, θ is the ratio of adsorbed enrofloxacin, K is the adsorption constant, and k' is the pseudo first-order rate constant. Thus, the relationship between $\ln(c/c_0)$ and t was shown in Fig. 6(b). According to the Fig. 6(b), the photocatalytic degradation of enrofloxacin followed the first-order reaction kinetics. The degradation rates of enrofloxacin with 10 wt%, 25 wt% or 50 wt% GaOOH/ZnBiTaO₅ as a photocatalyst was 0.01264 min⁻¹, 0.01431 min⁻¹ or 0.01279 min⁻¹, respectively, which was higher than that of pure ZnBiTaO₅ (0.01048 min⁻¹), pure GaOOH (0.00757 min⁻¹), or TiO₂ (0.00527 min⁻¹). It could be concluded that the construction of GaOOH/ZnBiTaO₅ heterojunction photocatalyst enhanced the photocatalytic performance of both pure ZnBiTaO₅ and pure GaOOH. In addition, the TOC data were used to analyse the mineralization rate of enrofloxacin with 25 wt% GaOOH/ZnBiTaO₅ as a photocatalyst, as shown in Fig. 6(c). After the illumination for 60 min, the mineralization rate of enrofloxacin was 27.38%, which was lower than the removal rate (58.27%) of enrofloxacin with 25 wt% GaOOH/ZnBiTaO₅ as a photocatalyst. This showed that in the photocatalytic process, enrofloxacin was not completely mineralized, and some intermediate products were produced.

Moreover, when 25 wt% GaOOH/ZnBiTaO₅ was used as a photocatalyst, the three-dimensional fluorescence changes of enrofloxacin during photocatalytic degradation was determined, as shown in Fig. 7. It could be observed that the colour of the three-dimensional fluorescence centre of enrofloxacin became lighter as the photocatalytic reaction time increased, indicating that enrofloxacin was gradually removed during photocatalysis.

The reusability was one of the important indicators for evaluating photocatalytic activity of photocatalyst. Fig. 8(a) shows the cyclic photocatalytic degradation of enrofloxacin with 25 wt% GaOOH/ZnBiTaO₅ heterojunction as a photocatalyst. As shown in Fig. 8(a), the removal rate of enrofloxacin decreased by

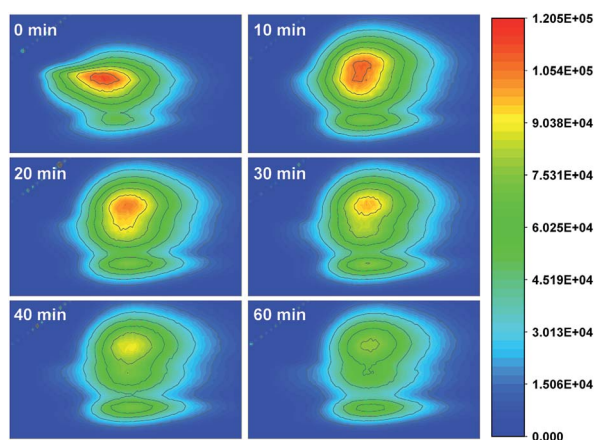


Fig. 7 The three-dimensional fluorescence changes of enrofloxacin during photocatalytic degradation with 25 wt% GaOOH/ZnBiTaO₅ as a photocatalyst.

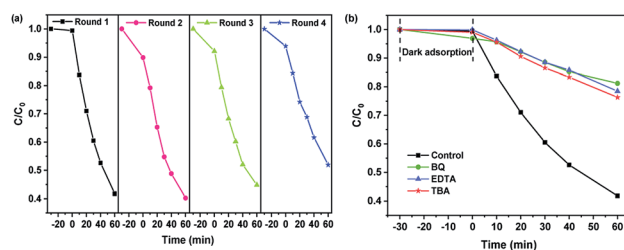


Fig. 8 Cyclic photocatalytic degradation of enrofloxacin with 25 wt% GaOOH/ZnBiTaO₅ as a photocatalyst (a); removal of enrofloxacin with the addition of different radical scavengers with 25 wt% GaOOH/ZnBiTaO₅ as a photocatalyst (b).

10.21% after four cycles. Fig. 8(b) shows the effect of radical scavengers on the degradation of enrofloxacin with 25 wt% GaOOH/ZnBiTaO₅ as a photocatalyst. The different radical scavengers were separately added to the enrofloxacin solution at the beginning of the photocatalytic experiment to determine the active species in the process of degrading enrofloxacin. The radical scavengers we used in this paper were ethylenediaminetetraacetic acid (EDTA), *tert*-butyl alcohol (TBA) and benzoquinone (BQ), which captured holes (h^+), hydroxyl radicals ($\cdot OH$) and superoxide radicals ($\cdot O_2^-$), respectively.^{51,52} The formulated EDTA, TBA or BQ concentration was 0.15 mmol L⁻¹, and the amount of EDTA, TBA or BQ added was 1 mL. According to Fig. 8(b), when the EDTA, TBA or BQ was added in enrofloxacin solution, the removal rate of enrofloxacin decreased by 36.73%, 34.57% or 39.46%, respectively, comparing with the control group. Therefore, it could be concluded that $\cdot O_2^-$, h^+ and $\cdot OH$ were all the active radicals during degrading enrofloxacin process.

In order to further confirm the presence of $\cdot O_2^-$ and $\cdot OH$ in the procedure of photocatalytic degradation, the EPR characterization was performed and the DMPO spin-trapping EPR spectra of 25 wt% GaOOH/ZnBiTaO₅ heterojunction photocatalyst was shown in Fig. 9. In the EPR characterization process, the 5,5-dimethyl-1-pyrroline *N*-oxide (DMPO) was used to spin traps the active radicals in the system for detection. As we could see from Fig. 9, when it was in darkness no EPR signals relevant to DMPO adducts were detected for 25 wt% GaOOH/ZnBiTaO₅ heterojunction photocatalyst. However, after ultraviolet light irradiation for 10 min, there were apparent signals in

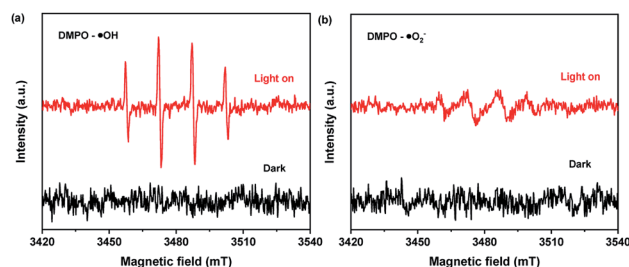


Fig. 9 DMPO spin-trapping EPR spectra of 25 wt% GaOOH/ZnBiTaO₅ heterojunction photocatalyst in aqueous dispersion for DMPO- $\cdot OH$ (a) and in methanol dispersion for DMPO- $\cdot O_2^-$ (b).



Fig. 9(a) and (b), which were corresponding with DMPO/ $\cdot\text{OH}$ adducts and DMPO/ $\cdot\text{O}_2^-$ adducts, respectively.^{53,54}

Possible degradation mechanism analysis

The possible photocatalytic degradation mechanism of enrofloxacin under illumination with GaOOH/ZnBiTaO₅ heterojunction photocatalyst is shown in Fig. 10. The potentials of the valence band (VB) and conductor band (CB) for semiconductor can be counted according to the eqn (7) and (8).⁵⁵

$$E_{\text{CB}} = X - E^{\circ} - 0.5E_{\text{g}} \quad (7)$$

$$E_{\text{VB}} = E_{\text{CB}} + E_{\text{g}} \quad (8)$$

where, E_{g} is the band gap of semiconductor, E° is the energy of free electrons on the hydrogen scale (about 4.5 eV), and X is the electronegativity of the semiconductor. According to the above equations, the potentials of VB and CB for GaOOH were counted to be 3.890 V and -0.870 V, respectively. The potentials of VB and CB for ZnBiTaO₅ were counted to be 3.265 V and 0.075 V, respectively. As shown in Fig. 10, when the GaOOH/ZnBiTaO₅ heterojunction was irradiated by ultraviolet light, both GaOOH and ZnBiTaO₅ absorbed light and internally generated electrons–holes pairs. The electrons on the CB of GaOOH could transferred to the CB of ZnBiTaO₅ and the holes on the VB of GaOOH could transferred to the VB of ZnBiTaO₅. Thus, the recombination of electrons and holes in the ZnBiTaO₅ was increased, which was agreement with the results of PL measurement. The CB of ZnBiTaO₅ was 0.075 V which was more positive than $\text{O}_2/\cdot\text{O}_2^-$ (-0.33 V). However, the CB of GaOOH was -0.87 V which was more negative than $\text{O}_2/\cdot\text{O}_2^-$ (-0.33 V). Thus, the electrons in the CB of GaOOH could convert O_2 to $\cdot\text{O}_2^-$ which degraded enrofloxacin, which was shown as path 1 in Fig. 10. In addition, the holes that came from the VB of GaOOH and ZnBiTaO₅ could convert OH^- that absorbed on the surface of photocatalyst to $\cdot\text{OH}$. Subsequently, the $\cdot\text{OH}$ degraded enrofloxacin. This was shown as path 2 in Fig. 10. Finally, the holes in the VB of GaOOH and ZnBiTaO₅ could directly oxidize and degrade enrofloxacin due to the strong oxidizing ability and

this was shown as path 3 in Fig. 10. Overall, the construction of GaOOH/ZnBiTaO₅ heterojunction had both positive and negative effect on ZnBiTaO₅. According to the results of degradation experiments, the construction of GaOOH/ZnBiTaO₅ heterojunction improved the photocatalytic performance of ZnBiTaO₅, so it was necessary to construct GaOOH/ZnBiTaO₅ heterojunction.

Conclusions

In this paper, pure ZnBiTaO₅ was synthesized by the solid-state reaction method firstly. The pure ZnBiTaO₅ crystallized with a pyrochlore-type structure, a cubic crystal system and a space group $Fm\bar{3}m$ and the lattice parameter of the pure ZnBiTaO₅ was calculated to be 5.268012 Å. Then, 10 wt%, 25 wt% and 50 wt% GaOOH/ZnBiTaO₅ heterojunction photocatalysts were synthesized by solvothermal method. The diffraction peaks of pure GaOOH and pure ZnBiTaO₅ were both observed in XRD results of 10 wt%, 25 wt% and 50 wt% GaOOH/ZnBiTaO₅ heterojunction photocatalysts, which meant that the 10 wt%, 25 wt% and 50 wt% GaOOH/ZnBiTaO₅ heterojunction photocatalysts were synthesized successfully. In addition, the construction of heterojunction structure increased the band gap of ZnBiTaO₅, according to the UV-Vis DRS results. In the experiments of degrading enrofloxacin, the removal rate of enrofloxacin with 10 wt%, 25 wt% or 50 wt% GaOOH/ZnBiTaO₅ as a photocatalyst was 57.02%, 58.27% or 54.55%, respectively, which was higher than that of pure ZnBiTaO₅ (53.7%), pure GaOOH (35.4%) or TiO₂ (29.37%). Therefore, the construction of heterojunction could improve the photocatalytic performance of pure ZnBiTaO₅ and pure GaOOH. Besides, it was confirmed that $\cdot\text{O}_2^-$, h^+ and $\cdot\text{OH}$ were all active radicals in degradation process. And the $\cdot\text{O}_2^-$ and $\cdot\text{OH}$ generated during photocatalytic process were determined by EPR. Finally, the possible paths of degradation of enrofloxacin were described in detail.

Conflicts of interest

There are no conflicts to declare.

Acknowledgements

This study was supported by a grant from the Research Foundation of Innovative Research and Supporting Program of Changchun Normal University in 2019, a grant from the Research Foundation of Science and Technology Bureau of Jilin Province for Middleaged Technological Innovative Scientist and Team Based on Environmental Function Material and Water Pollution Control, a grant from China–Israel Joint Research Program in Water Technology and Renewable Energy (No. 5), the National Natural Science Foundation of China (No. 20877040).

References

- 1 A. Fujishima, X. Zhang and D. A. Tryk, *Surf. Sci. Rep.*, 2008, 63(12), 515–582.

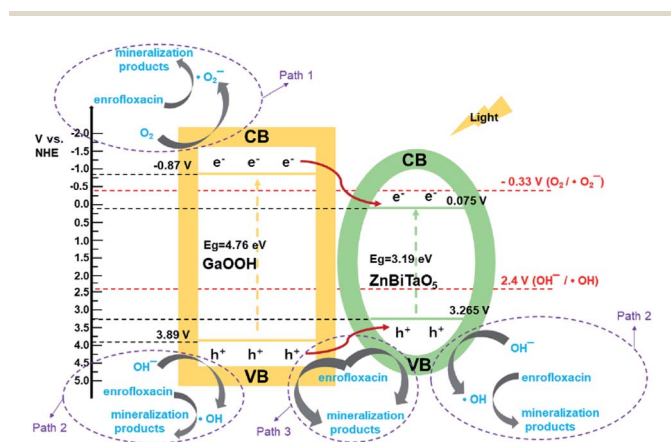


Fig. 10 Possible photocatalytic degradation mechanism of enrofloxacin under illumination with GaOOH/ZnBiTaO₅ heterojunction photocatalyst.



- 2 K. Hashimoto, H. Irie and A. Fujishima, *Jpn. J. Appl. Phys.*, 2005, **44**(12), 8269–8285.
- 3 A. Mills and S. L. Hunte, *J. Photochem. Photobiol., A*, 1997, **108**(1), 1–35.
- 4 A. L. Linsebigler, L. Guangquan, J. T. Yates and T. John, *Chem. Rev.*, 1995, **95**(3), 735–758.
- 5 S. Sakthivel and H. Kisch, *Angew. Chem., Int. Ed.*, 2010, **42**(40), 4908–4911.
- 6 M. R. Hoffmann, S. T. Martin, W. Choi, *et al.*, *Chem. Rev.*, 1995, **95**(1), 69–96.
- 7 D. Beydoun, R. Amal, G. Low, *et al.*, *J. Nanopart. Res.*, 1999, **1**(4), 439–458.
- 8 X. M. Zhou, G. Liu, J. G. Yu, *et al.*, *J. Mater. Chem.*, 2012, **22**(40), 21337–21354.
- 9 X. Zhang, Z. H. Ai, F. L. Jia, L. Z. Zhang, X. X. Fan and Z. G. Zou, *Mater. Chem. Phys.*, 2007, **103**, 162–167.
- 10 J. K. Zhou, Z. G. Zou, A. K. Ray and X. S. Zhao, *Ind. Eng. Chem. Res.*, 2007, **46**, 745–749.
- 11 G. K. Zhang, X. Zou, J. Gong, F. S. He, H. Zhang, Q. Zhang, Y. Liu, X. Yang and B. Hu, *J. Alloys Compd.*, 2006, **425**, 76–80.
- 12 K. W. Li, Y. Wang, H. Wang, M. K. Zhu and H. Yan, *Nanotechnology*, 2006, **17**, 4863–4867.
- 13 J. F. Luan, B. C. Pan, Y. Paz, Y. M. Li, X. S. Wu and Z. G. Zou, *Phys. Chem. Chem. Phys.*, 2009, **11**, 6289–6298.
- 14 J. Xu, Y. P. Wan, Y. L. Huang, Y. R. Wang, L. Qin and H. J. Seo, *Mater. Lett.*, 2016, **179**, 175–178.
- 15 A. A. Alemi, R. Kashfi and B. Shabani, *J. Mol. Catal. A: Chem.*, 2014, **392**, 290–298.
- 16 Y. Y. Bu, Z. Y. Chen and C. J. Sun, *Appl. Catal., B*, 2015, **179**, 363–371.
- 17 S. Nazim, T. Kousar, M. Shahid, M. A. Khan, G. Nasar, M. Sher and M. F. Warsi, *Ceram. Int.*, 2016, **42**, 7647–7654.
- 18 M. Kiransan, A. Khataee, S. Karaca and M. Sheydaei, *Spectrochim. Acta, Part A*, 2015, **140**, 465–473.
- 19 I. Ghaffar, M. F. Warsi, M. Shahid and I. Shakir, *Phys. E*, 2016, **79**, 1–7.
- 20 J. F. Luan, W. Zhao, J. W. Feng, H. L. Cai, Z. Zheng, B. C. Pan, X. S. Wu, Z. G. Zou and Y. M. Li, *J. Hazard. Mater.*, 2009, **164**, 781.
- 21 L. W. Zhang, H. B. Fu, C. Zhang and Y. F. Zhu, *J. Phys. Chem. C*, 2008, **112**, 3126–3133.
- 22 J. F. Luan and J. H. Chen, *Materials*, 2012, **5**, 2423–2438.
- 23 X. X. Xu, A. K. Azad and J. T. S. Irvine, *Catal. Today*, 2013, **199**, 22–26.
- 24 G. Carta, M. Casarin, N. El Habra, M. Natali, G. Rossetto, C. Sada, E. Tondello and P. Zanella, *Electrochim. Acta*, 2005, **50**, 4592–4599.
- 25 B. Cui, H. Lin, X. C. Zhao, J. B. Li and W. D. Li, *Acta Phys.-Chim. Sin.*, 2011, **27**, 2411–2415.
- 26 U. Lamdab, K. Wetchakun, S. Phanichphant, W. Kangwansupamonkon and N. Wetchakun, *J. Mater. Sci.*, 2015, **50**, 5788–5798.
- 27 S. K. Ray, D. Dhakal and S. W. Lee, *Chem. Eng. J.*, 2018, **347**, 836–848.
- 28 J. S. Cheng, L. Frezet, P. Bonnet and C. Wang, *Catal. Lett.*, 2018, **148**, 1281–1288.
- 29 L. M. Song, Y. M. Li, H. F. Tian, X. Q. Wu, S. Fang and S. J. Zhang, *Mater. Sci. Eng., B*, 2014, **189**, 70–75.
- 30 C. M. Yang, G. M. Gao, Z. F. Guo, L. T. Song, J. Z. Chi and S. C. Gan, *Appl. Surf. Sci.*, 2017, **400**, 365–374.
- 31 X. Liu, G. Qiu, Y. Zhao, N. Zhang and R. Yi, *J. Alloys Compd.*, 2007, **439**, 275–278.
- 32 M. Sun, D. Li, W. Zhang, X. Fu, Y. Shao, W. Li, G. Xiao and Y. He, *Nanotechnology*, 2010, **21**, 355601.
- 33 Y. Inoue, *Energy Environ. Sci.*, 2009, **2**, 364–386.
- 34 J. Sato, H. Kobayashi and Y. Inoue, *J. Phys. Chem. B*, 2003, **107**, 7970–7975.
- 35 M. Sun, D. Li, W. Zhang, X. Fu, Y. Shao, W. Li, G. Xiao and Y. He, *Nanotechnology*, 2010, **21**, 355601.
- 36 P. Q. Huang and J. F. Luan, *RSC Adv.*, 2019, **9**, 19930–19939.
- 37 Z. G. Zou, J. H. Ye and H. Arakawa, *J. Mater. Sci. Lett.*, 2000, **19**, 1909–1911.
- 38 S. Krehula, M. Ristić, S. Kubuki, Y. Iida, M. Fabián and S. Musić, *J. Alloys Compd.*, 2015, **620**, 217–227.
- 39 J. F. Luan, Y. Shen, S. Wang and N. B. Guo, *Polymers*, 2017, **9**, 69.
- 40 G. G. Li, C. Peng, C. X. Li, P. P. Yang, Z. Y. Hou, Y. Fan, Z. Y. Cheng and J. Lin, *Inorg. Chem.*, 2010, **49**, 1449–1457.
- 41 X. H. Liu, G. Z. Qiu, Y. Zhao, N. Zhang and R. Yi, *J. Alloys Compd.*, 2007, **439**, 275–278.
- 42 G. Deroubaix and P. Marcus, *Surf. Interface Anal.*, 1992, **18**, 39.
- 43 B. R. Strohmeier, *Surf. Sci. Spectra*, 1994, **3**, 128.
- 44 B. V. R. Chowdari and Z. Rong, *Solid State Ionics*, 1996, **86**, 527.
- 45 P. Kulkarni, S. K. Kulkarni, A. S. Nigavekar, S. K. Agarwal, V. P. S. Awana and A. V. Narlikar, *Phys. C*, 1990, **166**, 530.
- 46 G. R. Gruzalski and D. M. Zehner, *Phys. Rev. B: Condens. Matter Mater. Phys.*, 1986, **34**, 3841.
- 47 A. R. H. F. Ettema and C. Haas, *J. Phys.: Condens. Matter*, 1993, **5**, 3817.
- 48 G. Leonhardt, A. Berndtsson, J. Hedman, M. Klasson and R. Nilsson, *Phys. Status Solidi B*, 1973, **60**, 241.
- 49 B. J. Flinn and N. S. McIntyre, *Surf. Interface Anal.*, 1990, **15**, 19.
- 50 X. C. Meng and Z. S. Zhang, *Appl. Surf. Sci.*, 2017, **392**, 169–180.
- 51 R. Palominos, J. Freer, M. A. Mondaca and H. D. Mansilla, *J. Photochem. Photobiol., A*, 2008, **193**, 139–145.
- 52 Y. W. Gao, Y. Wang and H. Zhang, *Appl. Catal., B*, 2015, **178**, 29–36.
- 53 Y. Liu, S. Yu, Z. Y. Zhao, F. Dong, X. A. Dong and Y. Zhou, *J. Phys. Chem. C*, 2017, **121**(22), 12168–12177.
- 54 K. Liu, J. L. Li, X. Yan and W. D. Shi, *Nano*, 2017, **12**(10), 1750129.
- 55 L. Jiang, X. Yuan, G. Zeng, *et al.*, *Appl. Catal., B*, 2018, **227**, 376–385.

